# Auto-tuned Path-based Iterative Reconstruction (aPBIR) for X-ray Computed Tomography

Meng Wu, Andreas Maier, Yan Xia, and Rebecca Fahrig

***Abstract*—Model-based iterative reconstruction (MBIR) techniques have demonstrated many advantages in X-ray CT image reconstruction. The tuning parameter value in MBIR that regulates the strength of the penalty function is critical for achieving good reconstruction results but difficult to choose. The path-based iterative reconstruction (PBIR) method empowered by the path seeking algorithm is capable of efficiently generating a series of MBIR images with different strengths of the penalty function. In this paper, we present an approach to automatically select the tuning parameter value by finding the maximal separation between the noise reduction and the smoothing effects. Simulations shows that the proposed auto-tuned PBIR method produces images that are comparable to the hypothetically "best" MBIR image.**

***Index Terms*—CT, MBIR, Path seeking, PBIR**

## I. Introduction

The model-based iterative reconstruction (MBIR) method for 3D computed tomography (CT) has shown potential to improve image quality and reduce radiation dose [1]. The MBIR method is usually formulated in the Bayesian framework as a maximum a posteriori or maximum likelihood problem. However, the prior distribution of the object is unknown, and the maximum likelihood estimator is often ill-posed. A common solution is to add a constraint/regularization to the maximum likelihood model to formulate the penalized maximum likelihood problem. Over last two decades, extensive research has been conducted regarding the most suitable statistical model, penalty function, and acceleration techniques [2]–[4]. Moreover, choosing an appropriate strength of the penalty function, also as known as tuning parameter value, remains as one of the major difficulties of the MBIR method.

In this study, we consider the penalized weighted least-squares (PWLS) algorithm [2]

$$\mu = \underset{\mu \geq 0}{\operatorname{argmin}} \frac{1}{2} \sum_i w_i ([P\mu]_i - l_i)^2 + \beta h(\mu) \tag{1}$$

where $P$ denotes the system matrix for the data acquisition geometry, $l_i$ denotes the logged normalized projection of the $i$th ray, and $w$ is the least-squares weight to account for the noise level in the X-ray projection data. Function $h(\mu)$ is the penalty function (also known as regularization), $\mu$ is the reconstruction image, and $\beta$ is the tuning parameter that regulates the strength of the penalty function. In this paper, we used the penalized least-squares notation for simplicity

$$\begin{aligned} \text{minimize} \quad & \frac{1}{2}\|A\mu - y\|_2^2 + \beta h(\mu) = g(\mu) + \beta h(\mu) \\ \text{subject to} \quad & \mu \geq 0, \end{aligned} \tag{2}$$

where $A = W^{1/2}P$, $y = W^{1/2}l$, and $g(\mu)$ denotes the least-squares part. $W$ is the diagonal matrix containing $w_i$. It is well known that the value of the tuning parameter is critical to the reconstruction results [5], [6]. For example, if $\beta$ is too small, the regularization is not strong enough to suppress noise and artifacts; if $\beta$ is too big, the image is over blurred and even exhibits patchy behavior. In fact, the values of the tuning parameter ($\beta$) produce a series of reconstruction images indexed by $\beta$ value.

To the best of our knowledge, there is no perfect way to choose the tuning parameter value that would lead to the reconstruction with maximum clinical utility. Instead of focusing on a single optimal tuning parameters, the path-based iteration reconstruction (PBIR) method utilizes path seeking algorithms to efficiently compute the entire reconstruction path that covers all possible tuning parameter values [7], [8]. The PBIR method can provide complete information for a given reconstruction model, but still does not complete the task of finding the optimal tuning parameter. In this paper, we proposed a novel method to automatically select the tuning parameter that maximally separates the denoising and the smoothing effects.

## II. Methods

### A. Direction-of-gradient path seeking

We first present a path seeking algorithm that uses the direction of one gradient function to constrain the optimization problem thereby encouraging the image to change in the desired direction. For example, if we want to seek the path of increasing strength of the penalty function $h(\mu)$, then we would like to encourage the optimization updates (i.e. gradient descent) to go in the same direction as the $\nabla h(\mu)$. Let us consider adding a linear inequality constraint to the penalized least-squares problem as

$$\begin{aligned} \text{minimize} \quad & g(\mu) + \beta_1 h(\mu) \\ \text{subject to} \quad & \mu \geq 0 \\ & (\mu_j - \hat{\mu}_j) \cdot \nabla_j h(\hat{\mu}) \leq 0 \quad \forall j, \end{aligned} \tag{3}$$

where

$$\hat{\mu} = \underset{\mu \geq 0}{\operatorname{argmin}} \quad g(\mu) + \beta_1 h(\mu). \tag{4}$$

M. Wu, and R. Fahrig are with the Department of Radiology, Stanford University, USA e-mail:mengwu@stanford.edu.

A. Maier and Y. Xia are with Pattern Recognition Lab, Friedrich-Alexander University of Erlangen-Nuremberg, Germany.

TABLE I: Pseudo code for the path seeking algorithm.

Set $\beta = \beta_1$
Reconstruct an image $x = x_{\beta_1}$
For k = 1, 2, 3, ...
1) $s^{(k+1)} = \rho A^T(A\mu^{(k)} - y) + (1-\rho)v^{(k)}$.
2) If recently increase $\beta$, use a) otherwise use b).
a) Direction-of-gradient path seeking

$$\mu^{(k+1)} = \text{argmin}\beta h(\mu) + \frac{\rho}{2t}\|\mu - \mu^{(k)} + s^{(k+1)}\|_2^2$$
$$\text{subject to} \quad \mu \geq 0$$
$$(\mu_j - \mu_j^{(k)}) \cdot \nabla_j h(\mu^{(k)}) \leq 0 \quad \forall j$$

b) Standard ADMM step

$$\mu^{(k+1)} = \text{argmin}\beta h(\mu) + \frac{\rho}{2t}\|\mu - \mu^{(k)} + s^{(k+1)}\|_2^2$$
$$\text{subject to} \quad \mu \geq 0$$

3) $v^{(k+1)} = \frac{\rho}{\rho+1}A^T(A\mu^{(k+1)} - y) + \frac{1}{\rho+1}v^{(k)}$
4) If $\|x - x_{\beta_1}\|$ is not increasing, then record $x$ and increase $\beta$.
Until $\beta = \beta_2$.

The second linear inequality constraint in Eqn. (3) is inactive because the $\hat{\mu}$ is already optimal for the nonnegative constrained penalized least-squares problem.

If we slightly increase $\beta_1$ to $\beta_2$ in the direction-of-gradient constrained penalized least-squares problem (3) as

$$\begin{aligned} \text{minimize} \quad & g(\mu) + \beta_2 h(\mu) \\ \text{subject to} \quad & \mu \geq 0 \\ & (\mu_j - \hat{\mu}_j) \cdot \nabla_j h(\hat{\mu}) \leq 0 \quad \forall j \end{aligned} \tag{5}$$

and keep the $\hat{\mu}$ same as in Eqn. (4), the new solution will be suboptimal for the penalized least-squares problem (2) with $\beta_2$. But the solution of the problem (3) is still close to the solution of the reconstruction problem because increasing the strength of $h(\mu)$ and the direction-of-gradient constraint have very similar effects. To solve the direction-of-gradient constrained problem (3), we can simply apply a projection onto convex sets (POCS) step [3]. The POCS step will encourage updates of the image that favor minimizing $h(\mu)$, which increases the path seeking efficiency within the optimization framework.

It is not computationally efficient to compute the direction-of-gradient constrained problem (5), which only gives an approximation to the path image at each new $\beta$. We can merge the direction-of-gradient step into an efficient optimization solver such as the alternating direction method of multiplier (ADMM) [4]. To adapt the direction-of-gradient optimization, we can add the POCS in the denoising step of the ADMM algorithm. Additional ordinary ADMM steps can be used to improve the accuracy of the path seeking. The direction-of-gradient based path seeking algorithm is summarized in Table I.

For the direction-of-gradient based method, the path seeking is inside the framework of the constrained optimization problem that is more robust to ordered subset errors than the fixed step size update [9]. A suitable number of ordered subsets for the direction-of-gradient path seeking method is between 10 and 20. In order to execute alternatively between the normal and modified ADMM optimization steps, the additional optimization steps need to have the same number of ordered subsets [4], [9].

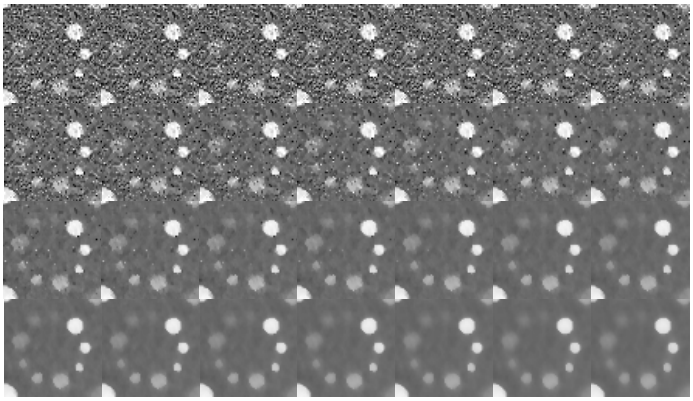

(a) Reconstruction path

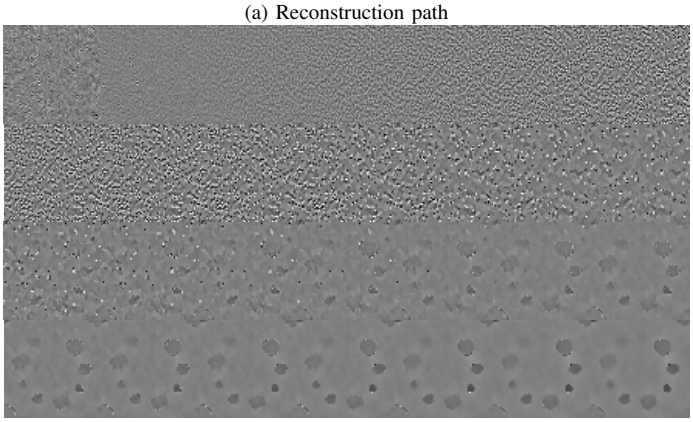

(b) Differences between two consecutive frames

Fig. 1: (a) Twenty eight path images of a 5 cm $\times$ 5 cm region-of-interest in the PWLS reconstruction path. The display window is [-50 150] HU. (b) Difference images between each two consecutive path images. The display window is [-10 10] HU.

### *B. Automatic tuning*

The path seeking algorithm can efficiently compute the reconstruction path, but the task of selecting the optimal tuning parameter value is not completed. Because the entire reconstruction path is already available, one way to choose the appropriate tuning parameter is to apply a numeric metric to those path images and select the frame (or tuning parameter) with the highest score. However, the numeric metric has to be suitable for the clinical task, which is an open research question. In this paper, we present a generic way of selecting the tuning parameter that has maximal separation of noise reduction and smoothing.

Figure 1 (a) shows an example of 28 frames in the MBIR reconstruction path using the path seeking method. The sequence of images changes from noisy to over smoothed. Figure 1 (b) shows the corresponding difference images between each

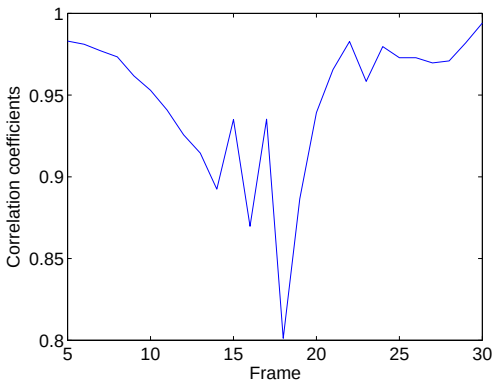


(a)

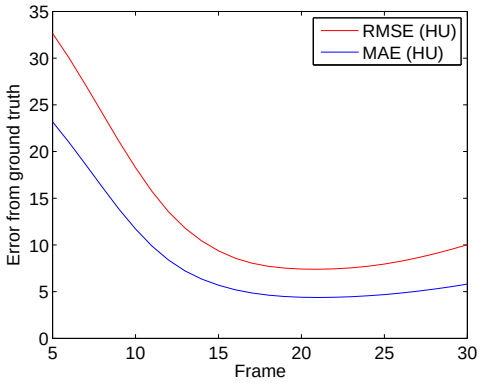


(b)

Fig. 2: (a) Correlation coefficients between two consecutive difference images. (b) RMSE and MAE between each path image and ground truth.

two consecutive path images in Figure 1(a). The effects of changing the penalty function strength are now presented in the difference images. When the tuning parameter is small, increasing the strength of the penalty function mainly reduces the noise in the reconstructions. In the first row of difference images, the changes are uniform throughout the region-of-interest (ROI), and there is no clear structure of the phantom. As the noise level in the reconstructions becomes low (end of the second row), the penalty function starts to influence the shape and value of the soft tissue patterns.

As shown in Figure 1(b), the changes in the first half of the reconstruction path correspond to the noise reduction, and the changes in the second half of the reconstruction path correspond to the smoothing. If we compute the correlation coefficients between each two consecutive difference images, there are high correlations inside the first and second halves as shown in Figure 2(a). At the 18th frame, the correlation coefficient drops because the changes caused by the noise is independent to the structure. Therefore, the corresponding frame implies the maximal separation between the noise reduction and the smoothing effects. Figure 2 (b) shows the root-mean-square-error (RMSE) and the mean-absolute-error (MAE) between each path image and ground truth. The RMSE and MAE both have minimum values around the 18th frame, which validate our assumption. Then, we can apply the same approach to each small regions of the entire image

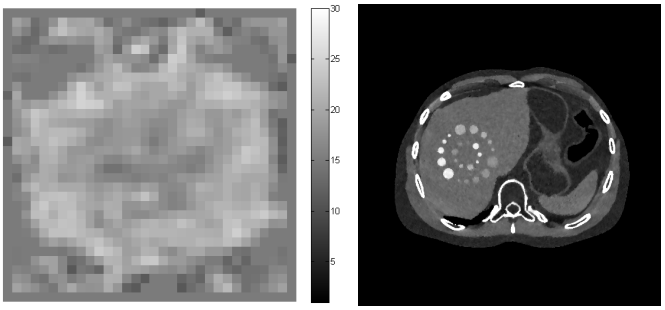


(a) (b)

Fig. 3: (a) Selected ROI frame indices used for optimal tuning parameter selection;. (b) Example of resulting aPBIR image.

to adaptively select optimal tuning parameters (Figure 3). The final auto-tuned PBIR (aPBIR) image is produced by stitching the regions with selected frame from the reconstruction path. In our experiments, we found a region size of 32×32 pixels (2.5 cm×2.5 cm) provides a good trade-off between noise and local structure.

## III. Simulations

A typical 64-slice diagnostic CT geometry was used in the simulations. A full circular rotation scan was performed over 360 degrees, containing 984 projections with the size of 888×64 pixels. The reconstructed image size 512×512×30 with in-plane spacing of 0.8×0.8 mm$^2$, and the slice thickness is 1 mm.

An abdomen XCAT phantom with added soft tissue patterns was used in this work. The phantom spacing of the XCAT phantom is 0.6 mm isotropic. The projection data were simulated in an axial scanning mode using a 120 kVp polychromatic spectrum. Simulated projections of the XCAT phantom were generated assuming an exposure of approximately 100 mAs and 50 mAs.

The simulated projection data are reconstructed using the penalized weighted least-squares (PWLS) method. We used the convex edge-preserving Huber function as the penalty function for image roughness. The transition value from quadratic to linear regions is set to 1, 5, and, 10 Hounsfield units (HU), respectively. The proposed path seeking methods were used to generate path images of the PWLS reconstruction with 30 $\beta$ values. The range of tuning parameters produces reconstructions ranging from very noisy to over smoothed.

## IV. Results

Figure 4 shows aPBIR reconstructions with different the Huber function (different transition values) at two different dose levels. With the automatically tuned parameter, the reconstructions show a good balance between noise reduction and smoothing. There is no visible white noise in the images. The images with the 1 HU Huber function (similar to total variation) exhibit some patchy behavior, and the soft tissue patterns are distorted. When using the 10 HU Huber function, the soft tissue background has more high frequency structures. The shapes of soft tissue contrast patterns in the liver are better preserved by the 10 HU Huber function. There is no

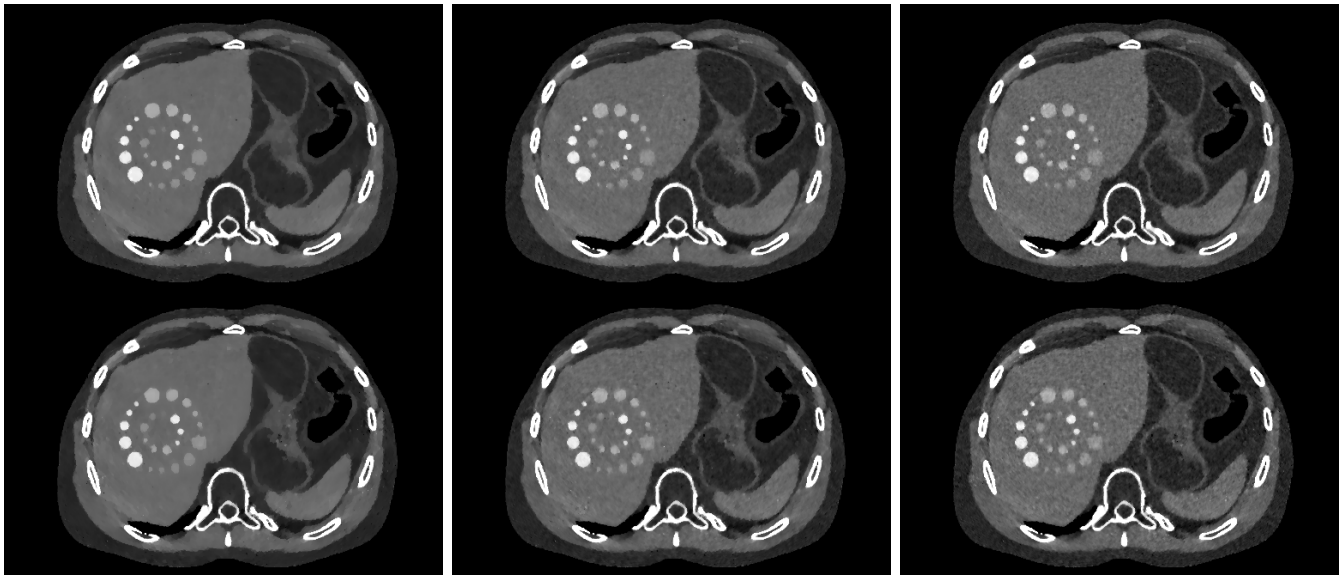

Fig. 4: Reconstruction results of the proposed aPBIR method. The first row uses 100 mAs data, the second row uses 50 mAs data. The columns from left to right correspond to the Huber function with transition values of 1, 5, and, 10 HU, respectively. The display window is [-50 150] HU.

TABLE II: RMSE and MAE measurements of the proposed aPBIR reconstructions in Figure 4 against the ground truth. The measurements for MBIR reconstructions used the image of on the reconstruction with the smallest values.

| Dose level (mAs) | 100 | 100 | 100 | 50 | 50 | 50 |
|---|---|---|---|---|---|---|
| Huber parameter (HU) | 1 | 5 | 10 | 1 | 5 | 10 |
| aPBIR RMSE (HU) | 28.2 | 28.2 | 28.4 | 29.0 | 29.2 | 29.3 |
| MBIR RMSE (HU) | 28.3 | 28.3 | 28.4 | 29.2 | 29.2 | 29.4 |
| aPBIR MAE (HU) | 8.24 | 8.59 | 9.04 | 8.51 | 8.93 | 9.46 |
| MBIR MAE (HU) | 8.19 | 8.41 | 8.63 | 8.51 | 8.79 | 9.05 |

obvious visual difference between 100 mAs and 50 mAs reconstructions, although 50 mAs reconstructions have more pepper noise, and the soft tissue patterns are more likely to be distorted.

Table II shows the comparison of RMSE and MAE measurements between the proposed aPBIR method and the "best" MBIR reconstructions. With the path seeking algorithm, we are able to obtain the reconstruction path of MBIR, and then compute the smallest RMSE and MAE values along the path. Therefore, the error measurements of the MBIR are the smallest values for the given reconstruction model. Note that, those values are unknown in practice because there is not ground truth. The aPBIR images have even slightly smaller RMSE than the "best" MBIR, because the tuning parameters are adaptively selected for different regions. The MAE measurements for aPBIR method are slightly larger than the "best" MBIR. Our simulation included beam hardening and partial volume effects, so the error measurements will not go down to zero. In addition, the path seeking algorithm not only permits efficient calculation of reconstructions for monotonically changing tuning parameter, but can also be used to investigate the impact of changing parameters in the penalty function itself.

## V. Conclusion

In this paper, we present an approach to automatically select the tuning parameter in iterative reconstruction by finding the maximum separation between noise reduction and smoothing effects. Simulation results show the proposed auto-tuned PBIR produces images that are comparable to the hypothetically "best" MBIR images. Future work will comprise validation of the algorithm in the clinical datasets. The present paper, however, indicates the feasibility of automatically selecting the tuning parameter using the aPBIR method.

## References


[1] J.-B. Thibault, K. D. Sauer, C. A. Bouman, and J. Hsieh, "A three-dimensional statistical approach to improved image quality for multislice helical CT," *Med. Phys.*, vol. 34, no. 11, p. 4526, 2007.

[2] I. A. Elbakri and J. A. Fessler, "Statistical image reconstruction for polyenergetic X-ray computed tomography," *IEEE Trans. Med. Imaging*, vol. 21, pp. 89–99, feb 2002.

[3] E. Y. Sidky and X. Pan, "Image reconstruction in circular cone-beam computed tomography by constrained, total-variation minimization.," *Phys. Med. Biol.*, vol. 53, no. 17, pp. 4777–4807, 2008.

[4] H. Nien and J. A. Fessler, "Fast X-Ray CT Image Reconstruction Using a Linearized Augmented Lagrangian Method With Ordered Subsets," *IEEE Trans. Med. Imaging*, vol. 34, pp. 388–399, feb 2015.

[5] J. Tang, B. E. Nett, and G.-H. Chen, "Performance comparison between total variation (TV)-based compressed sensing and statistical iterative reconstruction algorithms.," *Phys. Med. Biol.*, vol. 54, no. 19, pp. 5781–5804, 2009.

[6] A. S. Wang, J. W. Stayman, Y. Otake, G. Kleinszig, S. Vogt, G. L. Gallia, a. J. Khanna, and J. H. Siewerdsen, "Soft-tissue imaging with C-arm cone-beam CT using statistical reconstruction.," *Phys. Med. Biol.*, vol. 59, no. 4, pp. 1005–1026, 2014.

[7] M. Wu, Q. Yang, A. Maier, and R. Fahrig, "Approximate Path Seeking for Statistical Iterative Reconstruction," in *Proc. SPIE Med. Imaging*, pp. 9412–46, 2015.

[8] M. Wu, A. Maier, Q. Yang, and R. Fahrig, "Improve Path Seeking Accuracy for Iterative Reconstruction Using the Karush-Kuhn-Tucker Conditions," in *Intl. Mtg. Fully 3D Image Recon. Rad.*, (New Port, RI), pp. 248 – 251, 2015.

[9] M. Wu, A. Maier, Q. Yang, and R. Fahrig, "Path-based Iterative Reconstruction (PBIR) for X-ray Computed Tomography," arXiv:1512, pp. 1–10, 2015.